

# Conjoined Pyro-Piezoelectric Effect for Self-Powered Simultaneous Temperature and Pressure Sensing

Kai Song, Rudai Zhao, Zhong Lin Wang,\* and Ya Yang\*

**Ferroelectric materials use both the pyroelectric effect and piezoelectric effect for energy conversion. A ferroelectric BaTiO<sub>3</sub>-based pyro-piezoelectric sensor system is demonstrated to detect temperature and pressure simultaneously. The voltage signal of the device is found to enhance with increasing temperature difference with a sensitivity of about 0.048 V °C<sup>-1</sup> and with applied pressure with a sensitivity of about 0.044 V kPa<sup>-1</sup>. Moreover, no interference appears in the output voltage signals when piezoelectricity and pyroelectricity are conjoined in the device. A novel 4 × 4 array sensor system is developed to sense real-time temperature and pressure variations induced by a finger. This system has potential applications in machine intelligence and man-machine interaction.**

With the growing demand for new energy and functional devices, it is crucial to develop stable, sustainable, and smart electronics.<sup>[1–7]</sup> A wide variety of high-performance materials, which are utilized to fabricate functional devices based on photovoltaic effect,<sup>[8–10]</sup> piezoelectricity,<sup>[11,12]</sup> and thermoelectricity,<sup>[13,14]</sup> are attracting researchers' attention. Recently, ferroelectrics<sup>[15–19]</sup> with a complex perovskite structure, such as Pb(Zr,Ti)O<sub>3</sub>,<sup>[20,21]</sup> BiFeO<sub>3</sub>,<sup>[22,23]</sup> BaTiO<sub>3</sub>(BTO),<sup>[24–26]</sup> etc., have been reported to make significant improvements in light, heat, and pressure detecting. Most of these transducers can only detect a single source of energy, resulting in high cost and low

power conversion efficiency, which can largely limit their applications. Therefore, new approaches to develop multifunctional sensors are necessary, which are capable of sensing multiple physical variation signals simultaneously, without energy loss and signal interference. Moreover, making sensors to be more integrated and intelligent has become a trend in the current research worldwide.<sup>[27,28]</sup> A few research groups have investigated temperature and pressure sensors made from flexible polymer layers, which are based on changes in resistance<sup>[29,30]</sup> or combined with FET structure<sup>[31]</sup> as e-skin. However, there are no report about the conjoined pyro-piezo-

effect of ferroelectric materials as self-powered and integrated devices to detect external environmental changes for realizing simultaneous multisignals sensing.

Here we designed a 4 × 4 sensing array system based on eco-friendly BTO ferroelectric material. A BTO ceramic with Ag electrodes on both sides was designed as each sensing array unit. The coating of PDMS can make the device integrated and flexible, showing potential applications as portable and wearable electronics. The ferroelectric BaTiO<sub>3</sub> with superior properties of pyroelectricity and piezoelectricity exhibits remarkable sensitivity to both the temperature and strain, which can be utilized to detect individual temperature and pressure precisely.<sup>[32,33]</sup> The conjunction between pyroelectric and piezoelectric effects has been realized with “1 + 1 = 2” advantages, which is important for simultaneously detecting the temperature and pressure in one device. Each sensing array unit can work independently and synchronously without mutual interferences. The voltage signals of 16 Ag/BTO/Ag sensing units were simultaneously recorded as a mapping image in real time. Moreover, the 4 × 4 Ag/BTO/Ag matrix has been utilized as a practical password system to identify different human behaviours. The applying heat and stress by human finger touching can be observed by analysing real-time output signals. The self-powered system can process commands given by one user with more than one finger or even more than one user, enlarging the possibility of applications. According to the statistic data of voltage outputs, each person has a unique behavior pattern corresponding to finger touching signals, which thus can be utilized as new-era password keyboards. This new type of sensing system will have potential applications in environmental sensors, human body sensors, and even intelligent sensors, with a promising prospect.


As illustrated in **Figure 1a**, BaTiO<sub>3</sub> nanoparticles with a diameter of 60 nm are uniform nanospheres. After being sintering at 1200 °C, X-ray diffraction (XRD) patterns illustrating

K. Song, R. Zhao, Prof. Z. L. Wang, Prof. Y. Yang  
CAS Center for Excellence in Nanoscience  
Beijing Key Laboratory of Micro-nano Energy and Sensor  
Beijing Institute of Nanoenergy and Nanosystems  
Chinese Academy of Sciences  
Beijing 100083, P. R. China  
E-mail: yayang@binn.cas.cn

K. Song, R. Zhao, Prof. Z. L. Wang, Prof. Y. Yang  
School of Nanoscience and Technology  
University of Chinese Academy of Sciences  
Beijing 100049, P. R. China

Prof. Z. L. Wang  
School of Material Science and Engineering  
Georgia Institute of Technology  
Atlanta, GA 30332-0245, USA  
E-mail: zhong.wang@mse.gatech.edu

Prof. Y. Yang  
Center on Nanoenergy Research  
School of Physical Science and Technology  
Guangxi University  
Nanning, Guangxi 530004, P. R. China

 The ORCID identification number(s) for the author(s) of this article can be found under <https://doi.org/10.1002/adma.201902831>.

DOI: 10.1002/adma.201902831

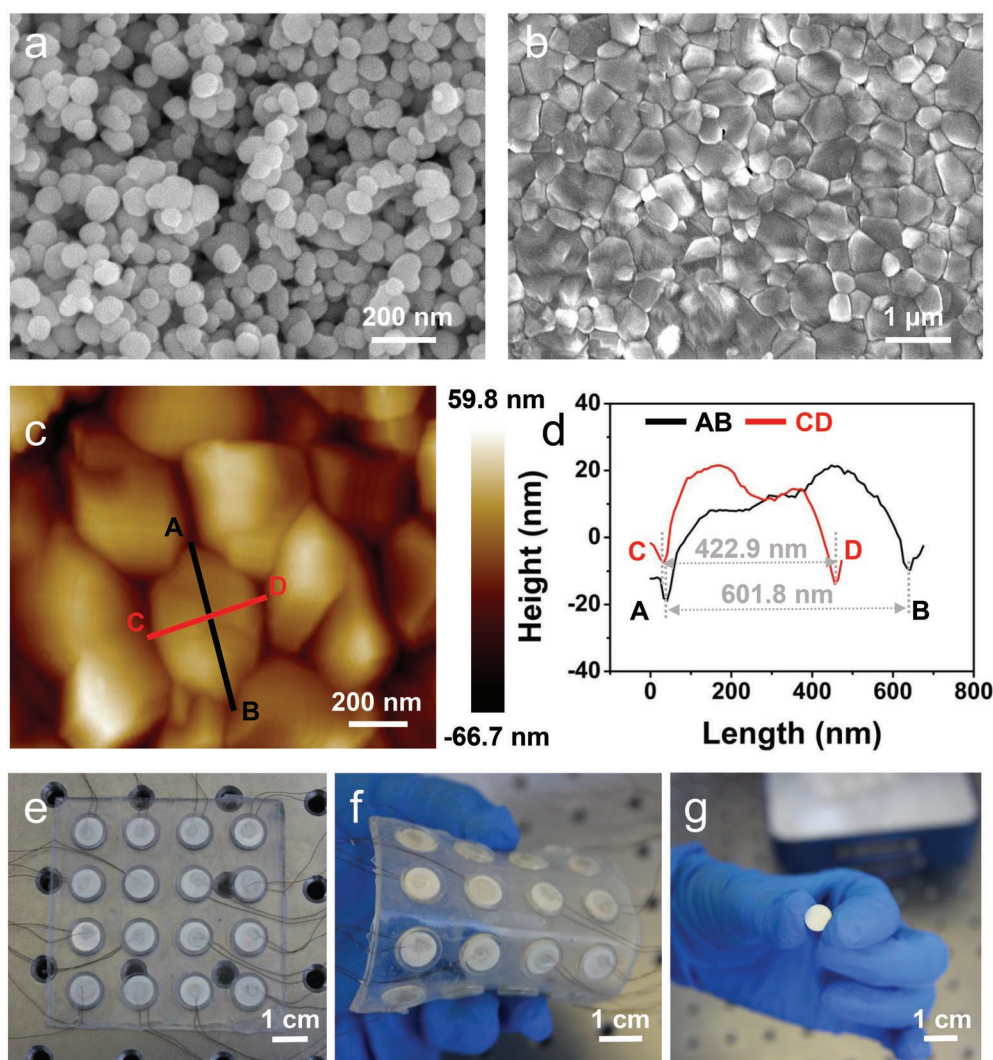


**Figure 1.** Characterization and photograph of BaTiO<sub>3</sub>(BTO) device. a) SEM image of BTO nanopowders. b) SEM image of BTO ceramic surface. c) AFM images of BTO ceramic surface. d) AFM topography scan of a BTO ceramic grain. e) Photograph of 4 × 4 pyro-piezo-electric sensing matrix. f) Photograph of bending 4 × 4 pyro-piezo-electric sensing matrix. g) Photograph of single Ag/BTO/Ag device.

the cubic phase (PDF #31-0174) of nanopowders were converted into the orthorhombic phase (PDF #81-2200) as shown in Figure S1 (Supporting Information). The ferroelectric properties of BaTiO<sub>3</sub> were derived from the phase transition, where orthorhombic phase exhibits spontaneous polarity instead of cubic phase.<sup>[34,35]</sup> Dense and compact BTO ceramic surface was investigated by scanning electron microscopy (SEM) in Figure 1b. The average grain size of the specimen was 500–800 nm. A typical BTO crystal particle was characterized by atomic force microscopy (AFM) in Figure 1c. It can be seen that the length of grain is 601.8 nm and the width is 422.9 nm. The assembled device in Figure 1g was fabricated as the base unit of pyro-piezo-electric sensing matrix. The components comprise sputtered Ag film electrodes of both sides and a BTO bulk as a sensing unit. The measured piezoelectric coefficient  $d_{33}$  of BTO device was 350 pC/N by applying a 3 kV polarizing DC voltage. As illustrated in Figure 1e,f, the 4 × 4 arrays designed to be coated with PDMS silicon rubber were integrated and

flexible (Figure S2, Supporting Information). Flexible device can be bent at different angles to accommodate the changing testing environment. 16 units with two thin wires each one was connected with a multichannel test system to collect real-time sensing data.

The working principle of the Ag/BTO/Ag sensor is associated with pyroelectric effect and piezoelectric conjunction effect. As typical ferroelectrics, spontaneous polarization exists in orthorhombic BaTiO<sub>3</sub> material.<sup>[30]</sup> At an initial state, free electrons in Ag/BTO/Ag device are on equilibrium state, where electrons are neutral and no charges can flow. When temperature changes, relative displacement of positive and negative electrical charges appear in BTO leading to variation of spontaneous polarization. A potential drop is thus created, resulting in the electrons flowing in the device from the bottom electrode to the top electrode under short circuit condition and an electric potential under open circuit condition. Therefore, pyroelectric current and voltage signals can

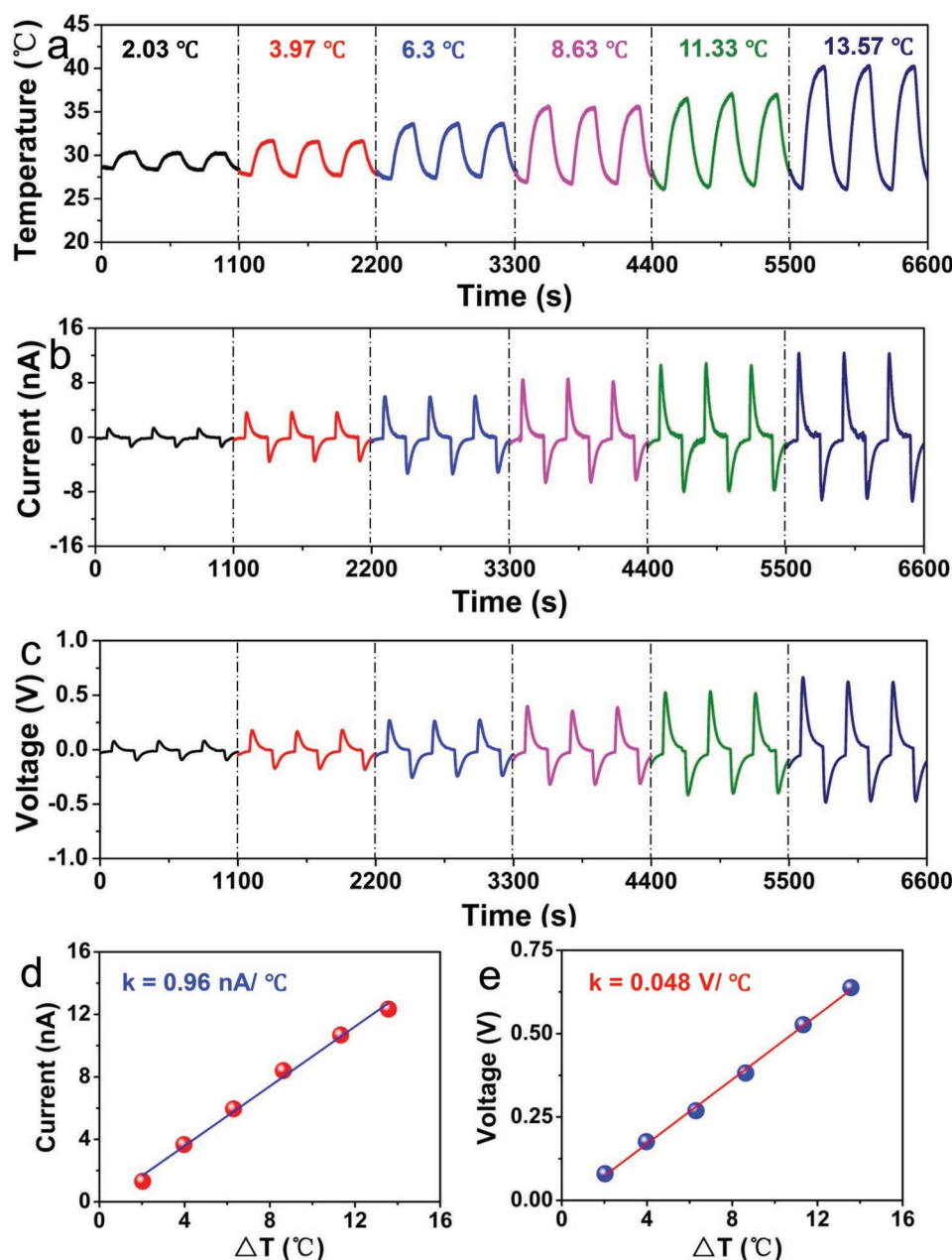


**Figure 2.** Pyroelectric properties of a single Ag/BTO/Ag sensing device. a) Measured temperature curves. b,c) Measured output current and voltage signals under different temperature gradients. d,e) Representative current and voltage values of device under the different temperature gradients.

be recorded by the test system. Moreover, the external pressure on the Ag/BTO/Ag structure can result in variation of spontaneous polarization owing to the noncentral symmetric crystalline structure. As a consequence, the piezoelectric voltage signals are measured. When heating and pressure conditions applied on the device together, pyro-piezoelectric effects coexist in BTO structure at the same time and interact with each other to enhance the flowing charge numbers, intensifying the multiple detections. Therefore, the intensive multisignals can be achieved to increase detection sensitivity and accuracy by pyro-piezo-electric conjunction effect.

The typical pyroelectric performances of the individual sensor unit are illustrated in **Figure 2**. The periodic heating conditions from 2.03 to 13.57 °C in Figure 2a are applied by using a semiconductor heater. The positive short-circuit current peak signals can be increased from 1.31 to 12.34 nA corresponding to heating variations as displayed in Figure 2b. Moreover, the positive peak voltage signals with a 100 M $\Omega$  loading resistance can be increased from 0.075 to 0.638 V. As depicted in Figure 2d,e, the standard current and voltage curves depending on heating temperature gradients present a perfectly reasonable linear relationship with a slope of 0.96 and 0.048. The standard current and voltage curves depending on cooling temperature

gradients are depicted in Figure S25e,f, respectively. Relying on sensing outputs curves, accurate temperature values can be detected. The negative current and voltage outputs with a 100 M $\Omega$  loading resistance under periodic cooling conditions are illustrated in Figure S6 (Supporting Information). While the device is in the heating state, the electric dipoles in BTO oscillate within a larger degree with their alignment axes, leading to a lower level of effective polarization. Thus, the quantity of induced charges in the electrodes is reduced, resulting in that electrons can flow from the bottom electrode to the top electrode. While the device is in the cooling state, the electric dipoles in BTO will oscillate within a smaller degree with their alignment axes, leading to a higher level of effective polarization. Thus, the quantity of induced charges in the electrodes is increased, resulting in an opposite movements of electrons in the circuit. So, the current directions of pyroelectric signals in heating and cooling states are opposite. We also investigated the pyroelectricity of traditional Ag/BTO/Ag structure without PDMS coating. Without PDMS coating, the heater has a direct contact with the Ag/BTO/Ag device, which can induce a faster temperature change. The pyroelectric current depends on the temperature change rate  $dT/dt$ , so the statistics (Figures S4–S5, Supporting Information) exhibit higher current and voltage signals of primary structure. However, it cannot be ignored that the lack of integration and flexibility reduces practicability. The standard curves of device without PDMS coating are illustrated in Figure S25a–d (Supporting Information). By the analysis of the curves and linear relationship slope, the device with PDMS coating is more stable when it was in heating and cooling conditions. We further verified each sensing unit of  $4 \times 4$  Ag/BTO/Ag matrix to detect temperature by using a multichannel data acquisition system. Several  $1 \text{ cm} \times 1 \text{ cm} \times 0.5 \text{ cm}$  cylindrical aluminum blocks underlying the array are utilized to conduct heat to units directly. The heating condition acting on the array with the shape of the letter “N” and “X” is demonstrated in infrared photographs of temperature distribution (Figure S7a,c, Supporting Information). Therefore, when the array is heated, measured corresponding outputs of each pixel are recorded by mapping images as shown in Figure S7b,d (Supporting Information). Mapping signals owing to pyroelectricity reveal each unit belonging to an integrated device can detect the temperature variations independently.

The electrical performances for the piezoelectric and pyro-piezo-electric conjunction effects are illustrated in Figure 3. Real-time responses from 0.059 to 0.58 V in Figure 3a are observed upon applying pressures from 15.4 to 27.6 kPa (Figure S9, Supporting Information). To eliminate the effect of triboelectric signals produced between force instrument surface and sensing device surface, an ultrathin PDMS film was stuck to the pressure surface of the force instrument. Objects of the same material generate little triboelectric charges when they contact each other and, therefore, no significant triboelectricity can appear. Three compressive strain cycles are counted three values of each pressure gradient. And the frequency of applying pressure is 2 Hz. As illustrated in Figure 3b, a fitting straight line with a slope of 0.044 is adapted to indicate that a high sensitivity of about  $0.044 \text{ V kPa}^{-1}$  and excellent linear voltage value curve depend on the compression gradients. Moreover, the cycle test from 15.4 to 27.6 kPa then to

15.4 kPa can indicate a good repeatability of pressure sensing (Figure S8, Supporting Information). In order to demonstrate the conjuncted pyro-piezo-electric properties of the device, the corresponding voltage outputs signals were measured under different stressing conditions and heating conditions. First, a continuous periodic temperature change is acted on the sensor. Without extraneous effects, the sharp pyroelectric voltage peak rose to 0.61 V. Starting with the second heating period, compression forces are applied as temperature changing ( $\Delta T = 13.57^\circ\text{C}$ ). As displayed in Figure 3c, the corresponding voltage peaks are remarkably observed, which can be increased from 0.74 to 1.06 V by increasing stress from 15.4 to 27.6 kPa. The result indicates that the enhancement of the output performance is associated with the conjuncted multiple effects. The responding time of transient conjuncted voltage is the same with pyroelectric responding time which represents no disturbance in multieffects. After instantaneous pyroelectricity from one-time heating disappears, piezoelectric outputs are still stable due to constant pressure changing. Furthermore, we analyzed statistical voltage values, as shown in Figure 3d, indicating that the voltage signals of the device can increase with increasing the temperature changes and the applied pressures. The correlation curves in Figure S10a (Supporting Information) under each heating conditions exhibit good linear dependency with increasing the applied pressures. Increasing the applied compression strain intensity on the device, the voltage signals of sensing pixel are enhanced. The corresponding increasing rates are depicted in Figure S26a (Supporting Information). Except for this heating condition ( $\Delta T = 13.57^\circ\text{C}$ ), when  $\Delta T = 2.03, 3.97, 6.3, 8.63, 11.33^\circ\text{C}$ , positive output signals (Figure S11, Supporting Information) can be also observed as increasing the pressure. As illustrated in Figures S15 and S16 (Supporting Information), initial pressure values increase with increasing heating temperature and decrease with increasing cooling temperature, which is associated with the deformations of PDMS coating layer. Although the deformation affected pressure initial value, the compressive stress is not compromised. Moreover, the negative output signals under cooling conditions ( $\Delta T = 1.8, 2.4, 3.8, 4.8, 5.8, 7.0^\circ\text{C}$ ) are displayed in Figure S12 (Supporting Information). What is interesting is that the corresponding negative voltage outputs are additive enhancement instead of reduction. The phenomenon indicates that the conjuncted effect can be realized to enhance output performances whether it is on heating or cooling state combined pressure state. To understand the multifunction of pyroelectricity and piezoelectricity further, the corresponding voltage signals were measured under different heating and cooling conditions with constant force change. As depicted in Figures S10b–d (Supporting Information), the corresponding voltage peaks are observed to increase from 0.45 to 1.09 V by increasing heating temperature variations from 2.03 to  $13.53^\circ\text{C}$ . The correlation curves under each force condition exhibits excellent linear dependency with increasing temperature. The corresponding increasing rates are depicted in Figure S26b (Supporting Information). Except for this pressure value ( $P = 27.6 \text{ kPa}$ ), when  $P = 15.4, 17.0, 19.2, 21.1, 24.9 \text{ kPa}$ , positive outputs (Figures S13–S14, Supporting Information) can be also displayed with increasing the pressure, as illustrated in Figures S17 and S18 (Supporting Information). The results

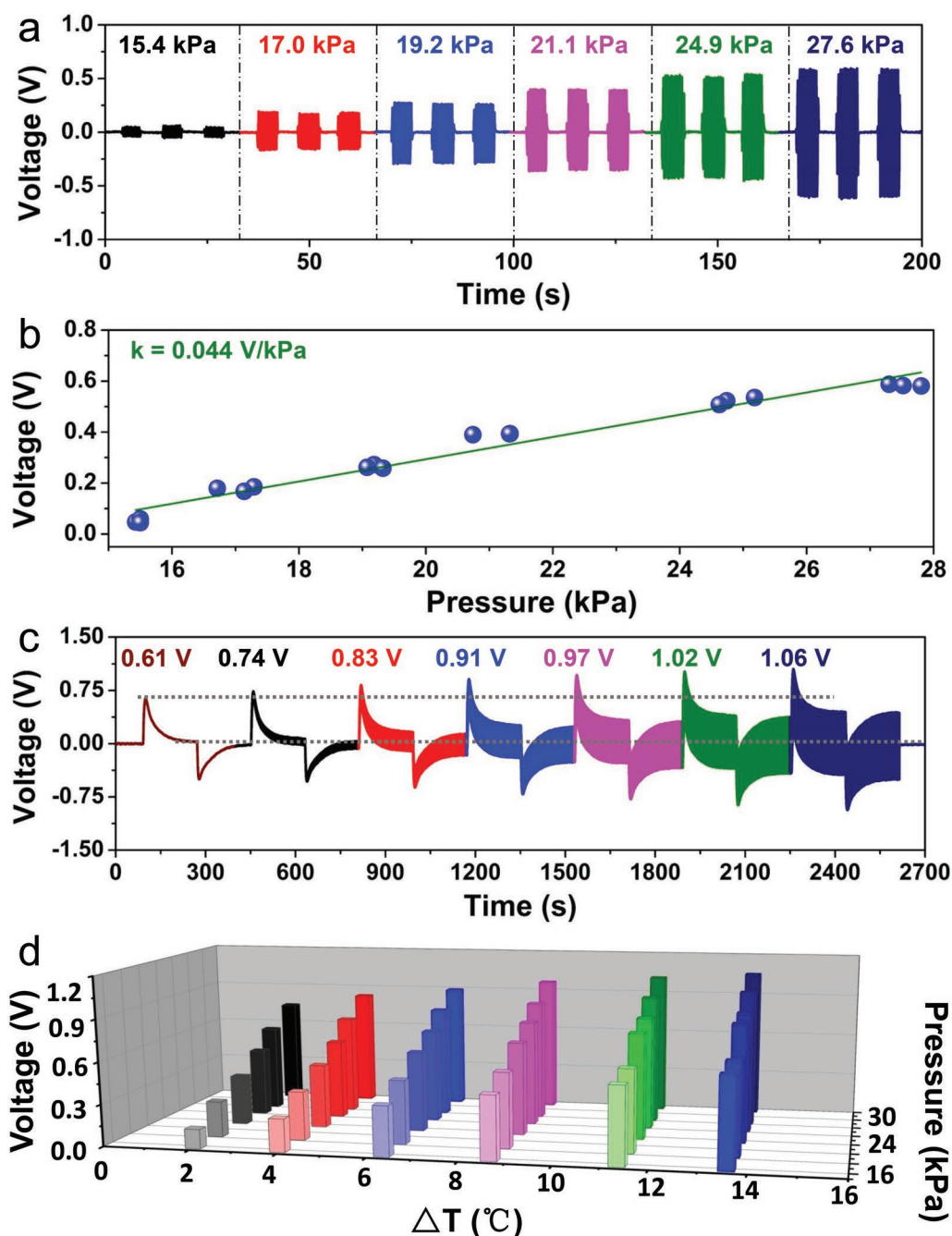


**Figure 3.** Piezoelectric and pyro-piezo-electric properties of single Ag/BTO/Ag sensing device. a) Measured voltage outputs corresponding to various pressure. b) Statistic voltage values dependence on pressure gradients. c) Measured voltage outputs when  $\Delta T = 13.57^\circ\text{C}$  in response to various pressure gradients. d) Bar graph of measured voltage values under different temperature gradients corresponding to various pressure.

indicate the existence of multifunctional effects can dramatically enhance the detection performances whenever only one effect exists.

To better research the conjuncted performances of Ag/BTO/Ag array by using the multieffects, further experiments are displayed in Figure 4. The representative curves of an Ag/BTO/Ag matrix unit induced by the simultaneously heating and pressing are demonstrated in Figure 4a. The corresponding pyroelectric voltage peak can be increased to 0.34 V

under heating condition ( $\Delta T = 8.63^\circ\text{C}$ ) and the corresponding piezoelectric voltage peak rose to 0.15 V under an applied pressure of 17 kPa. When both heating and pressure were applied on the device, the voltage peak can be increased to 0.49 V. The output values under both conditions are equal to the sum of values under heating and pressure individually. The results indicate that the sensing signals from different effects are conjuncted with enhancements without any energy loss. As shown in Figure S19 (Supporting Information), the response

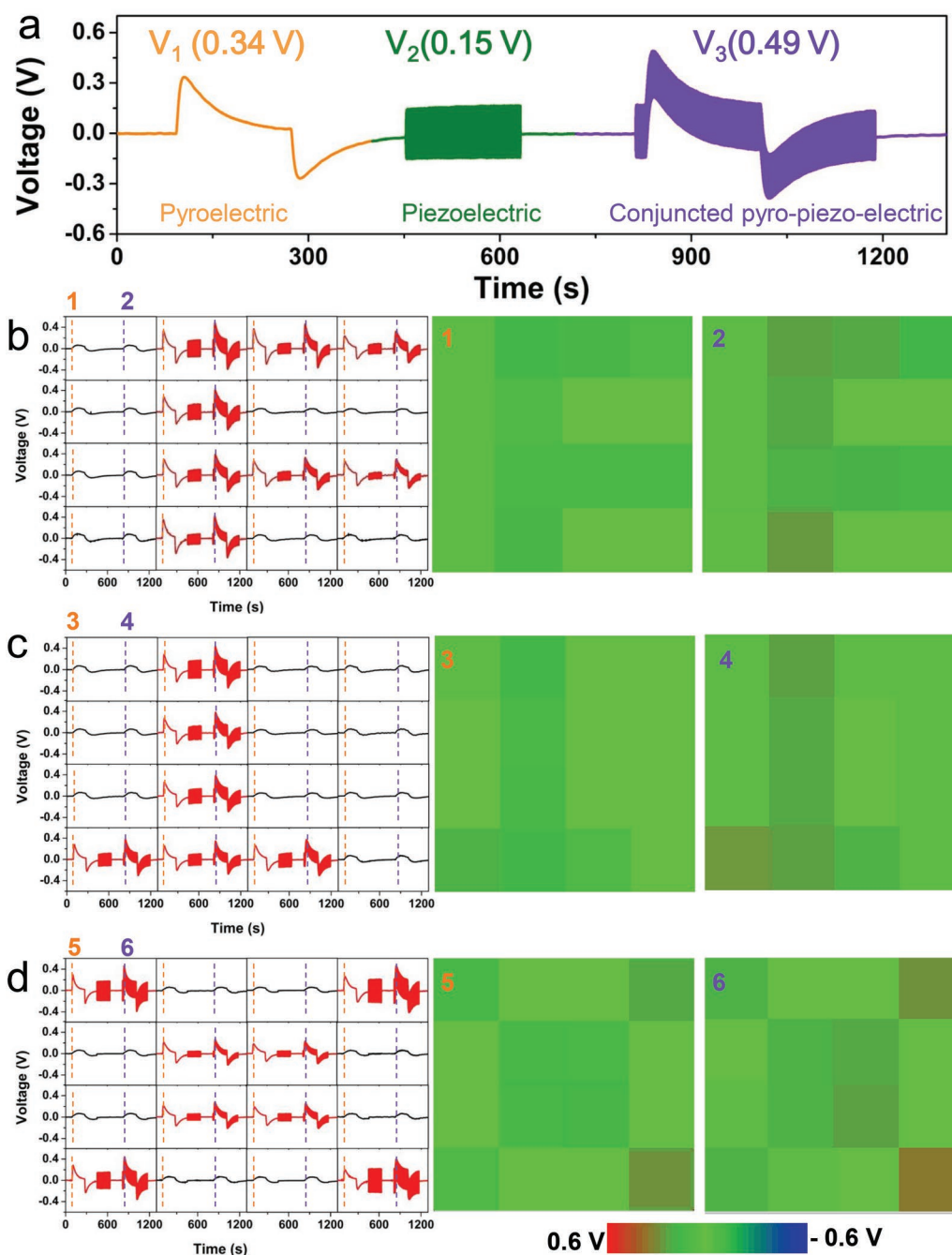


**Figure 4.** Pyro-piezo-electric properties of  $4 \times 4$  Ag/BTO/Ag sensing array. a) Output voltage change with individual temperature, pressure, and temperature–pressure conjuncted variety. b–d) Voltage curves of all pixels and corresponding voltage mapping images through different shapes. the shape of “Z” b) the shape of inverted “T” c) the shape of “X” d).

time of pyroelectric and piezoelectric output voltage are 8.6 and 0.24 s. The response time of pyro-piezo-electric signals is 7.8 s which is shorter than single pyroelectric. Figure 4b–d clearly displays the voltage output signal of each pixel unit and mapping images of different shapes under a heating condition, pressure condition, and conjuncted heating–pressure conditions. The shape of the letter “F”, the inverted letter “T”, and the letter “X” comprised of eight sensing units as corresponding pixels are applied to detect heat and pressure

change. Voltage mapping images of instantaneous pyroelectric signal marked as number “1”, “3”, “5”, and pyro-piezo-electric signal marked as number “2”, “4”, “6” can be distinguished that the color of pyro-piezo-electricity mapping images is deeper than pyroelectricity mapping images. Output voltages of each pixel unit revealed a consistent pattern that output values corresponding to multiple conditions are equal to the sum of values under heating and pressing condition individually.

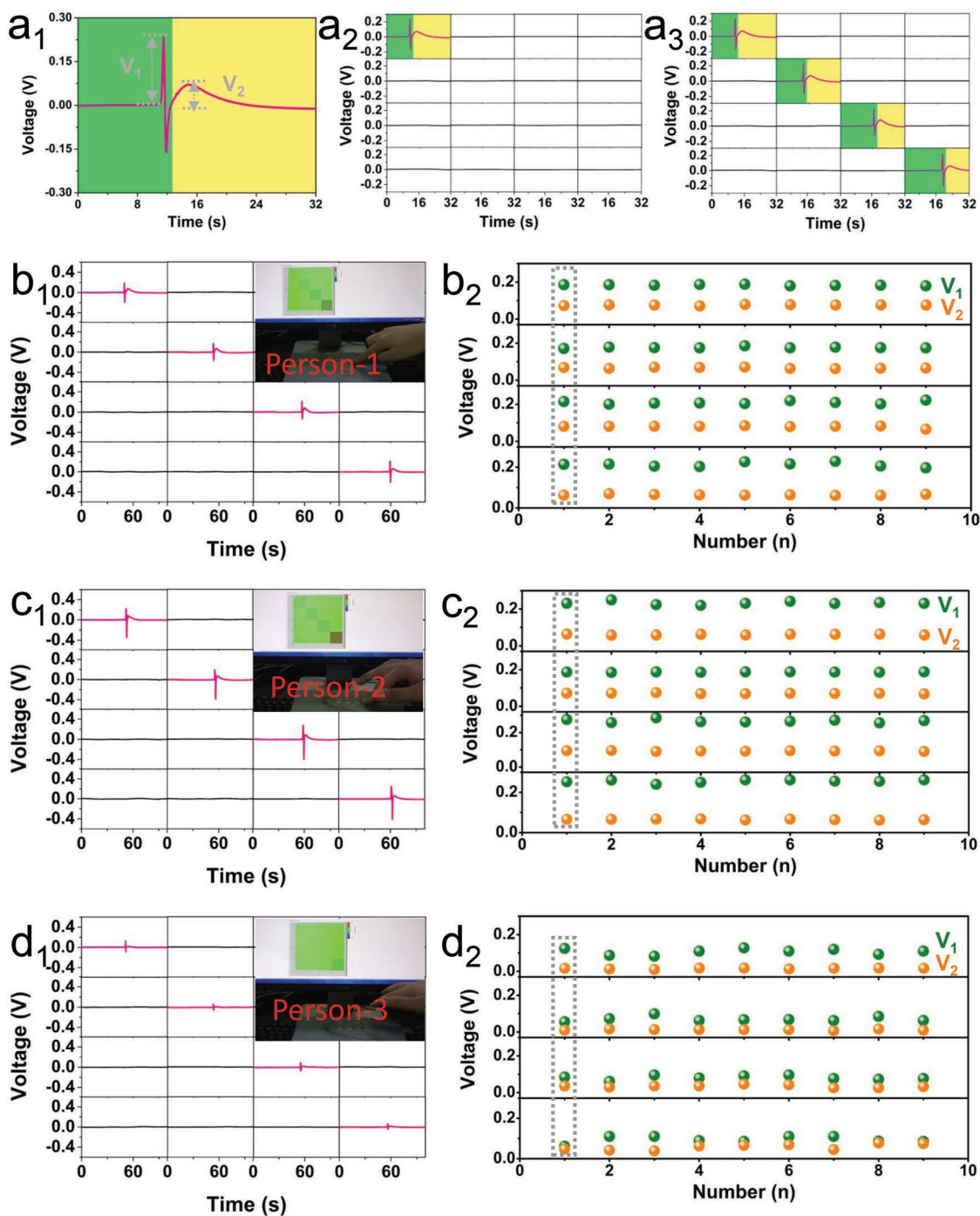


**Figure 5.** Finger signals recording by  $4 \times 4$  pyro-piezo-electric sensing matrix  $a_1$ – $a_3$ ) Typical output voltage curves and testing photographs as finger touching sensor units.  $b_1$ – $d_1$ ) Three characteristic voltage curves recorded from three testers.  $b_2$ – $d_2$ ) Three statistic sensing patterns corresponding to finger touching from three testers.

To illustrate the practical applications of Ag/BTO/Ag temperature–pressure sensor, the  $4 \times 4$  matrix of Ag/BTO/Ag device can be designed as a “password keyboard” (Figure S2b, Supporting Information). As a person typing passwords, the touching pressure and finger heat can be applied to the keyboard, which is a new method to design temperature–pressure sensor. Based on the human behaviors of entering passwords,

representative voltage signals are depicted in **Figure 5**. Two distinctive inductive signals can be detected in Figure 5a<sub>1</sub> as a forefinger touches one sensing array unit (Figure S21a, Supporting Information). The sharp voltage peak ( $V_1$ ) was generated by touching pressure up to 0.232 V and the gentle voltage peak ( $V_2$ ) was attributed to finger temperature heat up to 0.071 V. And the response time of pressing voltage peak ( $V_1$ )

is 0.32 s while the response time of heating voltage peak ( $V_2$ ) is 2 s. Except one finger sensing, voltage signals and mapping images as two fingers, three fingers, and four fingers touching the sensing units of array at the same time are shown in Figures S21b–d and S21f–h (Supporting Information). When the tester uses more than one finger to touch the device, the piezoelectricity values are lower than the value of one finger touching. Although the coated PDMS increased pyroelectric effect reaction time, the separated piezo-voltage and pyro-voltage peaks make touching signals more characteristic. The triboelectricity is based on contact electrification. When two different materials are in contact with each other, the negative and the positive static charges can be generated on the contact surfaces. When the contact surfaces are separated, the separation of positive and negative static charges will produce electric potential. The contact of the same material usually cannot produce triboelectricity. In order to exclude triboelectric signals produced between finger skin and PDMS surface of Ag/BTO/Ag device, the pyroelectric and piezoelectric peaks are presented in Figure S20a (Supporting Information) as a finger stuck to an ultrathin PDMS film pressing. The pure triboelectricity signals were measured when the finger pressed the device which was composed of unpoled Ag/BTO/Ag. The measured voltage signals (Figure S20b,c, Supporting Information) were produced by touching both sides of the unpoled device. The measured voltage signals (Figure S20d,e, Supporting Information) were obtained as touching both surfaces of the unpoled device by finger sticking to PDMS film. From the results, there are fewer impacts on pyro-piezo-electric effects whether the triboelectric effect coexists or not. The 1<sup>st</sup>, 6<sup>th</sup>, 11<sup>th</sup>, and 16<sup>th</sup> unit on the diagonal as four passwords are utilized to analyze touching pattern in Figure 5a<sub>3</sub>. Three typical typing patterns of three different testers are illustrated in Figure 5b<sub>1</sub>,c<sub>1</sub>,d<sub>1</sub> dynamically. According to the piezoelectric voltage ( $V_1$ ) and the former linear formula, the corresponding pressure values by three testers were calculated (person-1: 17.4 kPa, person-2: 18.2 kPa, person-3: 16.0 kPa). As seen from the real-time measuring photographs, mapping voltage images are displayed on a monitor screen. Piezoelectric values ( $V_1$ ) and pyroelectric values ( $V_2$ ) of nine times typing four sensing units on the diagonal by three persons are calculated in Figure 5b<sub>2</sub>,c<sub>2</sub>,d<sub>2</sub>. As compared with the signals between person-1 and person-2, the piezoelectric voltage values of person-2 are higher but the pyroelectric voltage values are lower than person-1, indicating that the pressure intensity of person-2 is larger and the finger staying time is longer of person-1. Moreover, the interval time between the two typing of person-2 is more than that of person-1. It can be seen that person-1 is typing faster than that of person-1. The pyroelectric voltage and piezoelectric voltage signals of person-3 are much less than other testers, so that person-3 has the smallest typing intensity and least staying time in the three testers. Although pyroelectric and piezoelectric signals of person-3 are minimal, the typing speed of person-3 as compared with other users is the fastest. Output data of each time by each person are exhibited in Figures S22–S24 (Supporting Information). Moreover, the corresponding output signals for the different 3 persons can also be seen in Video S1 (Supporting Information).

In summary, this article presents a novel design of pyro-piezo-electric conjunction sensing array via highly

responsive ferroelectric material. The voltage of the device was found to enhance with increasing temperature difference in time with a sensitivity of about 0.048 V °C<sup>-1</sup> or the applied pressure with a sensitivity of about 0.044 V kPa<sup>-1</sup>. The conjunction between pyroelectric and piezoelectric effects has been realized with “1 + 1 = 2”, which is important for simultaneously detecting the temperature and pressure in one device. Owing to no-loss and no-interference superposed multifunctions, every pixel unit of 4 × 4 matrix pyro-piezo-electric array system has been utilized to detect temperature and pressure simultaneously. Moreover, human finger touch sensing can be realized as intelligent identification. These investigations present a great potential application for future technologies such as smart sensors, intelligent compliant structures even man–machine interactive systems in progress.

## Experimental Section

**Fabrication of Ag/BTO/Ag Single Unit:** The BTO ceramic was made up of commercial BaTiO<sub>3</sub> nanopowders in Figure 1a (Aladdin industrial Corporation). 0.3 g BaTiO<sub>3</sub> powders were uniformly grinded with one drop of polyvinyl alcohol (2 wt%) which was used as a binder. A disk of 10 mm in diameter was pressed under 2 MPa pressure by an isostatic pressing machine. The molding samples were sintered in air at 1200 °C. The surfaces of sintered BTO ceramic were polished to thickness of about 850 μm by sandpapers. Ag thin film was sputtered as an electrode on both sides of BTO samples by DC magnetron sputtering. The Ag/BTO/Ag devices were poled at applied DC voltage of 3 kV for 30 min in an oil bath polarimeter.

**Fabrication of 4 × 4 Ag/BTO/Ag sensing array:** A 65 mm × 65 mm acrylic plate of thickness 2 mm punched 10 mm × 10 mm holes every 5 mm as a mold. The acrylic model was glued with 65 mm × 65 mm flexible Kapton film (Figure S2, Supporting Information). Prepolymer and crosslinker of PDMS elastomer (DC 184, Dow-Corning Corporation) were mixed in a weight ratio of 10:1. After degassing in a vacuum drying oven to be homogenous and bubble-free, the mixture was poured into 16 10 mm × 10 mm holes and heated at 80 °C for 2 h to solidify. Every single Ag/BTO/Ag device connected wires was put into each hole and coated with a new layer of PDMS. The thickness of PDMS layer was 0.8 mm. The acrylic mold was removed and 4 × 4 Ag/BTO/Ag sensing array was prepared.

**Characterization and Measurements:** The nanostructures of BaTiO<sub>3</sub> nanopowders and BaTiO<sub>3</sub> ceramic surface were analyzed by scanning electron microscopy (Nova NanoSEM 450). The crystal size and morphology of BaTiO<sub>3</sub> grain were characterized by atomic force microscopy (Dimension Icon, Bruker). The nanostructure and crystalline structure of BaTiO<sub>3</sub> were examined by X-ray diffraction with Cu Kα radiation (PANalytical X'Pert3 Powder). The  $d_{33}$  (piezoelectric constant) of Ag/BTO/Ag was measured by the quasi-static piezoelectric coefficient tester.

A semiconductor thermoelectric cooler system was utilized to supply temperature variations. An infrared thermal imaging device was used to record the temperature variations of the Ag/BTO/Ag sensing array. A low-frequency electrodynamic vibration shaker (Labworks Inc. pa151, sc-121) was used to provide pressure variations. The output pressure signals were recorded by force gauge (IMADA, ZTA-50N). The output current signals were measured by Stanford Research SR570. The voltage output signals and mapping images of the 4 × 4 array of Ag/BTO/Ag sensing device were simultaneously recorded by the multichannel dynamic test and analysis system NI PXIe-6358.

## Supporting Information

Supporting Information is available from the Wiley Online Library or from the author.

## Acknowledgements

This work was supported by the National Key R&D Program of China (Grant No. 2016YFA0202701), the National Natural Science Foundation of China (Grant No. 51472055), External Cooperation Program of BIC, Chinese Academy of Sciences (Grant No. 121411KYS820150028), the 2015 Annual Beijing Talents Fund (Grant No. 2015000021223ZK32), the Qingdao National Laboratory for Marine Science and Technology (No. 2017ASKJ01), and the University of Chinese Academy of Sciences (Grant No. Y8540XX2D2).

## Conflict of Interest

The authors declare no conflict of interest.

## Keywords

BaTiO<sub>3</sub>, piezoelectric effect, pyroelectric effect, sensors

Received: May 4, 2019

Revised: June 20, 2019

Published online: July 5, 2019

- [1] D. Kim, N. Lu, R. Ma, *Science* **2011**, 333, 838.
- [2] Y. W. Choi, D. Kang, P. V. Pikhitsa, T. Lee, S. M. Kim, G. Lee, D. Tahk, M. Choi, *Sci. Rep.* **2017**, 7, 40116.
- [3] S. Gong, W. Schwalb, Y. Wang, Y. Chen, Y. Tang, J. Si, B. Shirinzadeh, W. Cheng, *Nat. Commun.* **2014**, 5, 3132.
- [4] Y. Zang, F. Zhang, D. Huang, X. Gao, C. A. Di, D. Zhu, *Nat. Commun.* **2015**, 6, 6269.
- [5] T. Yamada, Y. Hayamizu, Y. Yamamoto, Y. Yomogida, A. Izadi-Najafabadi, D. N. Futaba, K. Hata, *Nat. Nanotechnol.* **2011**, 6, 296.
- [6] C. Pang, G. Y. Lee, T. I. Kim, S. M. Kim, H. N. Kim, S. H. Ahn, K. Y. Suh, *Nat. Mater.* **2012**, 11, 795.
- [7] F. Xia, H. Wang, Y. Jia, *Nat. Commun.* **2014**, 5, 4458.
- [8] X. Fang, Y. Bando, M. Liao, T. Zhai, U. K. Gautam, L. Li, Y. Koide, D. Golberg, *Adv. Funct. Mater.* **2010**, 20, 500.
- [9] T. Ji, Q. Liu, R. Zou, Y. Sun, K. Xu, L. Sang, M. Liao, Y. Koide, L. Yu, J. Hu, *Adv. Funct. Mater.* **2016**, 26, 1400.
- [10] W. Ouyang, F. Teng, X. Fang, *Adv. Funct. Mater.* **2018**, 28, 1707178.
- [11] E. F. Crawley, J. De Luis, *AIAA J.* **1987**, 25, 1373.
- [12] C. Pan, L. Dong, G. Zhu, S. Niu, R. Yu, Q. Yang, Y. Liu, Z. L. Wang, *Nat. Photonics* **2013**, 7, 752.
- [13] F. Zhang, Y. Zang, D. Huang, C. A. Di, D. Zhu, *Nat. Commun.* **2015**, 6, 8356.
- [14] D. Champier, *Energy Convers. Manage.* **2017**, 140, 167.
- [15] C. R. Bowen, J. Taylor, E. LeBoulbar, D. Zabek, A. Chauhan, R. Vaish, *Energy Environ. Sci.* **2014**, 7, 3836.
- [16] J. Chakraborty, C. Harnagea, M. Celikin, F. Rosei, R. Nechache, *Nat. Photonics* **2018**, 12, 271.
- [17] I. Grinberg, D. V. West, M. Torres, G. Gou, D. M. Stein, L. Wu, G. Chen, E. M. Gallo, A. R. Akbashev, P. K. Davies, J. E. Spanier, A. M. Rappe, *Nature* **2013**, 503, 509.
- [18] Y. Yuan, Z. Xiao, B. Yang, J. Huang, *J. Mater. Chem. A* **2014**, 2, 6027.
- [19] A. Kvasov, L. J. McGilly, J. Wang, Z. Shi, C. S. Sandu, T. Sluka, A. K. Tagantsev, N. Setter, *Nat. Commun.* **2016**, 7, 12136.
- [20] K. Song, N. Ma, Y. Yang, *Adv. Mater. Technol.* **2017**, 2, 1700221.
- [21] Y. Yang, S. Wang, Y. Zhang, Z. L. Wang, *Nano Lett.* **2012**, 12, 6408.
- [22] J. Qi, N. Ma, X. Ma, R. Adelung, Y. Yang, *ACS Appl. Mater. Interfaces* **2018**, 10, 13712.
- [23] F. Z. Lu You, L. Fang, *Sci. Adv.* **2018**, 4, eaat3438.
- [24] K. Zhao, B. Ouyang, Y. Yang, *iScience* **2018**, 3, 208.
- [25] Y. Ji, K. Zhang, Z. L. Wang, Y. Yang, *Energy Environ. Sci.* **2019**, 12, 1231.
- [26] B. K. Pandey, S. Dias, K. K. Nanda, S. B. Krupanidhi, *J. Appl. Phys.* **2017**, 122, 234502.
- [27] Q. He, Y. Wu, Z. Feng, C. Sun, W. Fan, Z. Zhou, K. Meng, E. Fan, J. Yang, *Nano Energy* **2019**, 59, 689.
- [28] Y. Chen, Y.-C. Wang, Y. Zhang, H. Zou, Z. Lin, G. Zhang, C. Zou, Z. L. Wang, *Adv. Energy Mater.* **2018**, 8, 1802159.
- [29] J. S. Lee, K. Shin, O. J. Cheong, J. H. Kim, J. Jang, *Sci. Rep.* **2015**, 5, 7887.
- [30] J. Park, M. Kim, Y. Lee, H. S. Lee, H. Ko, *Sci. Adv.* **2015**, 1, e1500661.
- [31] N. T. Tien, S. Jeon, D. Kim, J. B.-H. Tok, Z. Bao, N.-E. Lee, J.-J. Park, *Adv. Mater.* **2014**, 26, 796.
- [32] Y. Ji, K. Zhang, Y. Yang, *Adv. Sci.* **2018**, 5, 1700622.
- [33] C. R. Bowen, H. A. Kim, P. M. Weaver, S. Dunn, *Energy Environ. Sci.* **2014**, 7, 25.
- [34] Y. Guo, K. i. Kakimoto, H. Ohsato, *Appl. Phys. Lett.* **2004**, 85, 4121.
- [35] N. Ma, B. P. Zhang, W. G. Yang, D. Guo, *J. Eur. Ceram. Soc.* **2012**, 32, 1059.